Nanoscale

Accepted Manuscript

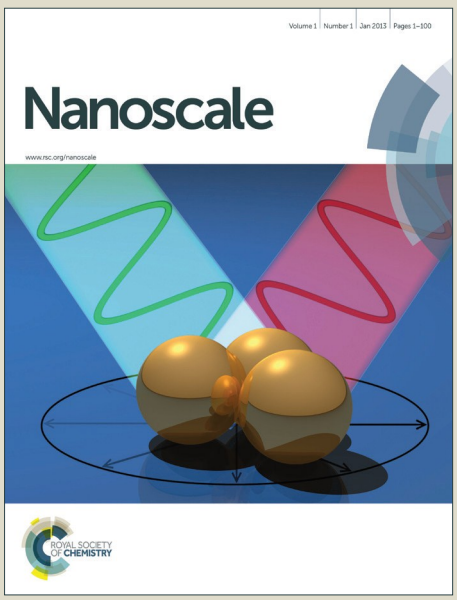

ROYAL SOCIETY OF CHEMISTRY

www.rsc.org/nanoscale

Nanoscale

COMMUNICATION

Utilizing the anti-ferromagnetic functionality of multiferroic shell to study exchange bias in hybrid core-shell nanostructures

Received 00th January 20xx,
Accepted 00th January 20xx

DOI: 10.1039/x0xx00000x

www.rsc.org/

S. S. Ali,[a,b] W. J. Li,[a] K. Javed,[a] D. W. Shi,[a] S. Riaz,[a,d] Y. Liu,[c] Y. G. Zhao,[c] G. J. Zhai,[b] and X. F. Han*[a]

A three-step method has been employed to synthesize 1D core-shell nanostructures consisting of ferromagnetic $Co_{90}Pt_{10}$ (CoPt) core and La doped multiferroic $Bi_{0.87}La_{0.13}FeO_3$ (BLFO) shell. La doping efficiently removes the secondary impurity phases in multiferroic shell and exchange interaction gives significant exchange bias effect demonstrating the anti-ferromagnetic functionality of $Bi_{0.87}La_{0.13}FeO_3$.

One-dimensional (1D) nanocylinders including nanowires (NWs) and nanotubes (NTs) have attracted considerable scientific interest during the last decade because of their significantly different novel structure and physical properties from thin films and their bulk counter parts.[1-3] From the application point of view, a great deal of attention has been paid to the synthesis and characterization of these nanostructures owing to their potential applications in sensors, microwave absorption, bio-logical separation and high density recording media.[4-7] Simultaneous existence of more than one ferroic orders such as ferromagnetic, ferroelectric and ferroelastic in multiferroics demonstrates significant technological promise in novel multifunctional devices. Switching in ferroelectric materials at the cost of electric field has already been proposed to design ferroelectric random access memories (FeRAM) containing the stored information in the form of remnant polarization.[8,9] It has been theoretically demonstrated that the mechanisms responsible for the ferroelectricity and magnetic ordering are mutually independent as the fact that ferroelectricity is associated with an empty outer shell d electrons while magnetic ordering is driven by the unpaired d or f electrons. These basic mutually exclusive in-compatibilities of multiferroics make them scarce to find as intrinsic materials with multi-functionalities and give rise to prepare artificial nanostructure with desired properties. For application point of view, the major constriction for single-phase magnetic ferroelectrics is the low magnetic ordering temperature. In such a scenario the best candidate is $BiFeO_3$ (BFO) with its perovskite structure because of its ferroelectric transition at about 1100 K and anti-ferromagnetic Néel temperature around 640 K are both well above the room temperature (RT).[10] Besides all these advantages, unfortunately, there are some inherent problems in BFO. Existence of parasitic phases during BFO synthesis is one of the culprits that tend to nucleate at grain boundaries and impurities. BFO is believed to be metastable at room temperature in air having impurities that appear during the sintering process. For thin film case, these impurities are known to improve the artificial remnant magnetization but very careful synthesis conditions are required to get rid of these impurities.[11-13] Through Mössbauer spectroscopy and neutron diffraction experiments, this compound is proved to be a G-type anti-ferromagnet with a spatially modulated spin structure. The macroscopic magnetization is cancelled by the incommensurate long-wavelength period which also puts constraints in realization of linear magneto-electric effects.[13,14] Another important issue is the leakage current owing to the presence of large number of charge centers that occur due to the existence of oxygen ion vacancies and Bi_2O_3 evaporation.[15] The above mentioned limitations are the main hindrance for the multifunctional device implementation of this compound and have been attempted by many researchers to resolve. One of the ways is the doping of rare earth lanthanide ions including La^{3+}, Nd^{3+}, Sm^{3+} or the divalent ions including Ca^{2+}, Sr^{2+}, Ba^{2+}, Pb^{2+} at the A site of BFO to replace Bi^{3+}.[16-20] Ferromagnetic behaviour in $BiFeO_3$ nanoparticles with small grain size up to 62 nm can be improved by destroying the spiral spin structure.[21,22] Since BFO presents a G-type anti-ferromagnetic order that can be exploited to modify the magnetization of a ferromagnet through exchange bias. In addition, the magnetization of an exchange-biased ferromagnet can be controlled with the manipulation in anti-ferromagnetic order in the presence of electric field owing to the existence of magnetoelectric coupling.[23-26]

[a] Beijing National Laboratory for Condensed Matter Physics, Institute of Physics, Chinese Academy of Sciences, Beijing 100190, China. E-mail: xfhan@iphy.ac.cn
[b] National Space Science Center, Chinese Academy of Sciences, Beijing 100190, China.
[c] Department of Physics and State Key Laboratory of Low-Dimensional Quantum Physics, Tsinghua University, Beijing 100084, China.
[d] Centre of Excellence in Solid State Physics, University of the Punjab, Lahore-54590, Pakistan
† Electronic Supplementary Information (ESI) available: See
DOI: 10.1039/x0xx00000x

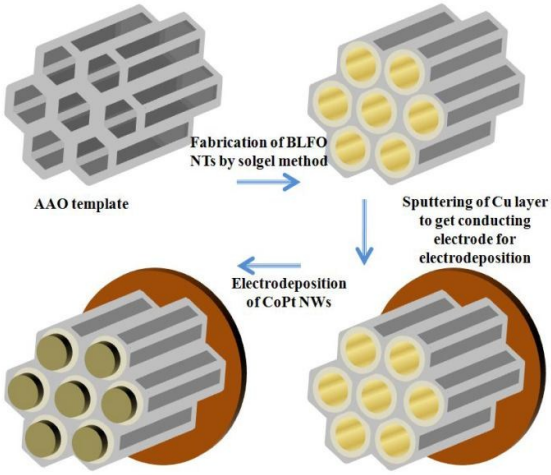

Fig. 1 AAO template assisted three-step route to synthesize CoPt-BLFO core-shell NWs.

In this work, we report low cost fabrication of 120 nm diameter well ordered hybrid core-shell NWs with ferromagnetic $Co_{90}Pt_{10}$ (CoPt) core and multiferroic $Bi_{0.87}La_{0.13}FeO_3$ (BLFO) shell followed by the study of their structural, magnetic and ferroelectric properties. Magnetic properties including magnetization reversal mechanism and specially exchange bias effect at room and low temperatures have been addressed in details in the light of anti-ferromagnetic ordering of BLFO shell. The highly ordered anodic aluminum oxide (AAO) templates are the best choice for the synthesis of 1D nanostructures because of their well aligned symmetry, uniform pore diameter and inter-pore distance. Besides the commercial availability, these templates can be fabricated by employing the two-step anodization process and the pore diameter can be tuned according to the requirement.

Fig. 1 shows detailed schematic demonstration of synthesis of double phase CoPt-BLFO core-shell NWs. The first step is to synthesize BLFO shell via sol-gel method, a template assisted growth. After getting well-aligned shells inside the template, a Cu layer is sputtered at one side to get conducting electrode followed by electrodeposition of CoPt core carried out via DC electrodeposition method. AAO templates with average pore diameter of about 120 nm have been used to synthesize BLFO NTs by sol-gel method and further electrodeposition of CoPt NWs inside the BLFO shell [ESI-1,2†]. Since the lack of infiltration causes porous NTs via sol-gel route therefore the immersion time of template into the sol has been adjusted with better reproducibility every time followed by a careful morphology analysis to get proper infiltration and sufficient wall thickness of about 20 nm [Fig. S1†].

The phase pure synthesis of $BiFeO_3$ is still a challenge due to high vulnerability of Bi and the existence of other more stable phases of bismuth ferrite [Fig. S2†]. The high volatility of Bi causes the other more stable phases to appear and results the lost of pure $BiFeO_3$ stoichiometry. To get rid of this problem, a suitable excessive amount of Bi has been added to the precursor. Since La substitution

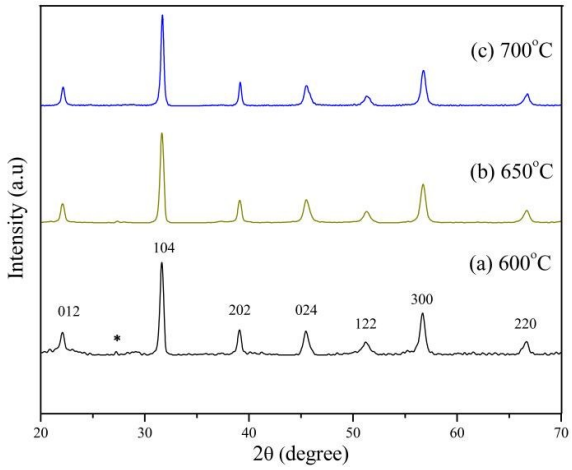

Fig. 2 XRD patterns of BLFO NTs annealed at different temperatures.

at the A site of BFO is an efficient way to improve the ferroelectric and ferromagnetic properties of BFO. Besides this, additionally it significantly reduces the volatilization of bismuth oxide and hence improves oxygen ion stability in the lattice.[22] A suitable amount of La has been added in precursor to fabricate $Bi_{0.87}La_{0.13}FeO_3$ NTs followed by the annealing at different temperatures to get best crystalline structure.

A complete etching of AAO template has been done in 1M solution of NaOH to get fine BLFO NTs for XRD analysis. Fig. 2 shows the XRD patterns of BLFO NTs taken after annealing at different temperatures with best polycrystalline peaks have been observed at 700˚C. A minor impurity phase of $Bi_2Fe_4O_9$ has been indicated with * which is removed at higher annealing temperatures. The standard XRD pattern 081-9950 with rhombohedral $Bi_{0.87}La_{0.13}FeO_3$ and space group R3c can be taken into account for comparison.

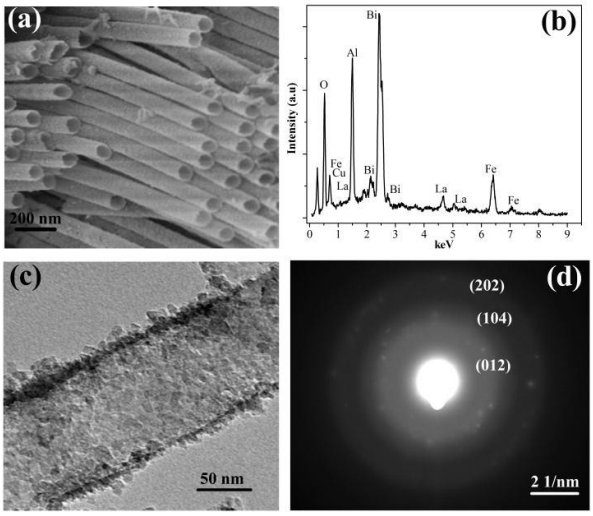

Fig. 3 (a) SEM image BLFO NTs after etching in NaOH solution. (b) EDS composition of BLFO NTs (c) TEM image of single BFLO NT after complete removal of AAO template. (d) SAED pattern of BLFO NTs indicating the polycrystalline structure.

The magnetic properties of BLFO NTs at room temperature have been measured by using vibrating sample magnetometer (VSM) [Fig. S3†]. Fig. 3a shows the scanning electron microscope (SEM) image of BLFO NTs with inner diameter of about 100 nm and wall thickness around 20 nm. Fig. 3b shows the energy dispersive spectrum (EDS) confirming the deposition of BLFO contents inside the pores via sol-gel method. The peaks of some other elements including Cu and Al are also appeared in the spectrum due to the use of copper tape for SEM analysis and incomplete etching of AAO template respectively. Fig. 3c illustrates the transmission electron microscope (TEM) image of single BLFO NT after complete removal of AAO template through etching in NaOH solution. Fig. 3d shows the selected area electron diffraction pattern (SAED) of BLFO NTs confirming the polycrystalline structure. AAO template assisted electrodeposition of transition metals and their alloys is a versatile method to synthesize magnetic NWs and NTs of tunable length and diameter with high aspect ratio.[27-29] AAO templates having nanopores filled with BLFO NTs by sol-gel method have been further employed for electrodeposition of CoPt core. A three electrode cell has been used potentiostatically at room temperature with constant stirring during electrodeposition [ESI-2†].

Fig. 4a shows the TEM image of CoPt-BLFO core-shell NW having 120 nm diameter with a clear observation of around 100 nm CoPt core and 20 nm wall thickness BLFO shell. A magnified view of interface between the ferromagnetic core and anti-ferromagnetic shell is shown in Fig. 4b. The SEM image of core-shell NWs taken after the partial removel of AAO template in NaOH solution is shown in Fig. 4c. The composition has been confirmed by EDS analysis as shown in Fig. 4d where the unnecessary peak of Al is appeared due to partial removel of AAO template.

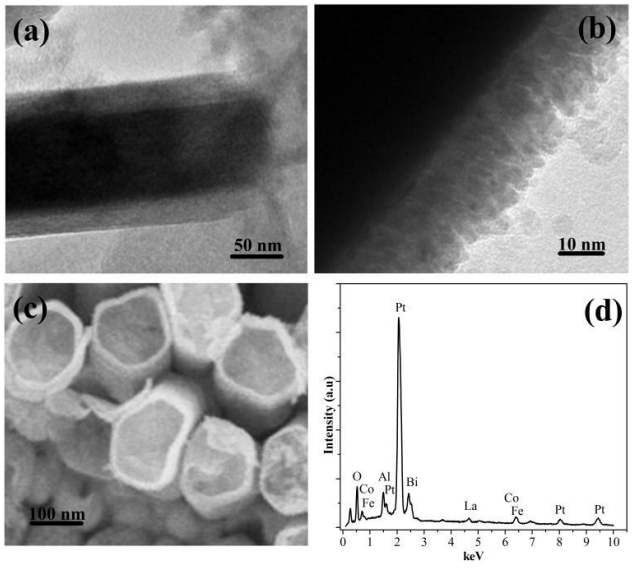

Fig. 4 (a-b) TEM images of CoPt-BLFO core shell NWs with 20 nm wall thickness of BLFO shell and 100 nm diameter of CoPt core. (c) SEM image of CoPt-BLFO core shell NWs after partial removal of AAO template. (d) CoPt-BLFO core shell NWs composition by EDS.

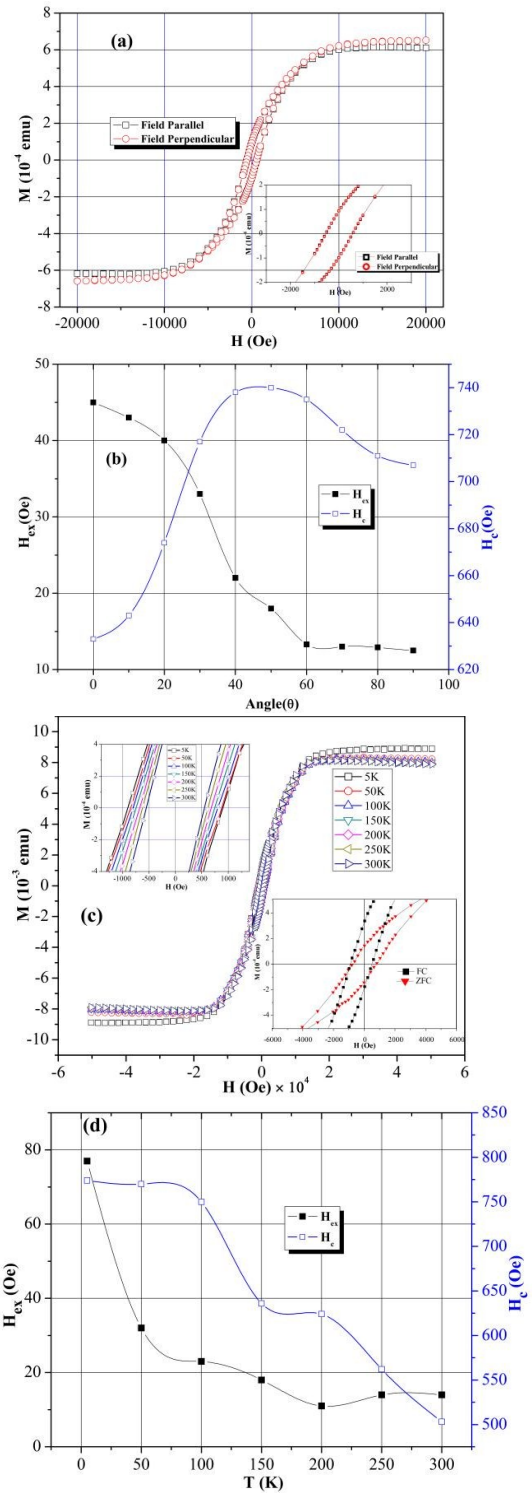

Fig. 5 (a) M-H loops of CoPt-BLFO core shell NWs measured at RT. (b) Angular dependence of coercivity and exchange bias in CoPt-BLFO core shell NWs. (c) Field cooled M-H loops of CoPt-BLFO core shell NWs with external magnetic field applied parallel to NWs axis. Bottom inset shows the FC and ZFC curves at 5 K. (d) Temperature dependence of coercivity and exchange bias in CoPt-BLFO core shell NWs after being field cooled.

Magnetic properties of core-shell CoPt-BLFO NWs are measured by VSM at room temperature and superconducting quantum interference device (SQUID) at lower temperatures. Fig. 5a shows the magnetic hysteresis loops of CoPt-BLFO core shell NWs with applied field in parallel and perpendicular directions to NWs axis gives a little different hysteresis loops. Since the NWs are closely packed in AAO template which leads to the stronger dipolar coupling among the wires, in such case the shape anisotropy is not as much dominent to induce easy magnetization axis sharply along the NWs axis. Another reason is that the length of NWs is a few μm which is an additional factor for the less dominency of shape anisotropy demonstrating a less anisotropic behaviour in our measurements. The alignment of easy magnetization axis is mainly depends on effective anisotropy field H_k. When the H_k value is positive i.e. $H_k > 0$, it gives a parallel alignment of easy magnetization axis with NWs axis wherease for the opposite case ($H_k < 0$) the easy magnetization axis alignment is perpendicular to NWs axis. The three major contributions in effective anisotropy field (H_k) are the shape anisotropy field ($2\pi Ms$), magnetostatic dipole interaction field and the magnetocrystalline anisotropy (H_{ma}) with first two mainly responsible for inducing easy magnetization axis along parallel and perpendicular to NWs axis, respectively.[30,31] The nanostructures synthesized by electrodeposition method are usually poly-crystalline or amorphous, for such nanostructures the magneto-crystalline anisotropy (H_{ma}) can be neglected.[32]

Fig. 5b shows the angular dependence of coercivity (H_c) and exchange bias (H_{ex}) in CoPt-BLFO core-shell NWs, where θ is the angle between the external magnetic field and the NWs axis. The two important magnetization reversal mechanisms in NWs and NTs are the curling and coherent rotation modes. A gradual increase in H_c has been observed leading to a peak value of 740 Oe at an angle of θ = 50° between the applied magnetic field and NWs axis. This increase in H_c with the increase in applied magnetic field angle corresponds to the curling mode of magnetization reversal mechanism. Later on there occurred a switching in magnetization reversal mechanism from curling to coherent showing a decrease in H_c from θ = 50° to θ = 90°. The competition between exchange energy and demagnetization energy mainly determines the magnetization reversal mechanism. According to curling model, the coherent mode can be dominent due to increase in exchange energy density with a decrease in size as there will be an increase in relative angle between neighboring moments. The other possibility is the increase in demagnetization energy density with the increase in aspect ratio which favours the curling mode. This is possibily due to a magnetization component along the hard axis, which causes an increase in demagnetization energy. In addition, the increase in aspect ratio may lead to introduce smaller domains which results in additional domain walls with a corresponding increase in demagnetization energy.[33] The threshold diameter between coherent rotation and curling is $d_c = 2\sqrt{A/M_s}$, where A is the exchange constant and M_s is the saturation magnetization. For wire diameters less then the critical diameter i.e. $d < d_c$ coherent rotation is dominant according to Stoner-Wohlfarth model[34], when the wire diameter (d) approaches the critical diameter (d_c), curling rotation occurs at smaller angles between the external magnetic field and NWs axis, whereas at larger angles it is switched to coherent, and for the case when wire diameter is larger than the critical diameter i.e. $d > d_c$, the curling rotation is dominant. The angular dependence of exchage bias (H_{ex}) is shown in Fig. 5b. The highest value of 45 Oe is observed at θ = 0° which is also the easy axis of magnetization in our case. With the increase in θ a gradual decrease occurs in H_{ex} to a minimum at θ = 90°. Although no magnetic field annealing has been employed in our measurements but indeed a clear existence of H_{ex} has been observed which is attributed to the rearrangement of anti-ferromagnetic domains in BLFO shell during the electrodeposition of ferromagnetic CoPt core. However, the exchange interactions can be significantly influenced by magnetic anisotropy, interface roughness, spin configuration and domains' orientation at the interface.[35] To study the temperature dependent magnetic properties of core-shell CoPt-BLFO NWs, M-H curves have been taken after being field cooled with 1000 Oe magnetic field from 300 K by using SQUID at temperatures T = 5, 50, 100, 150, 200, 250 and 300 K with magnetic field applied parallel to NWs' axis as shown in Fig. 5c. The bottom inset of Fig. 5c shows a comparison of field cooled and zero field cooled M-H curves taken at 5 K. At lower temperatures an increase in saturation magnetization (M_s) and the saturation field (H_s) is observed. The reduced thermal fluctuations cause significant contribution to surface magnetic moments resulting increased M_s values at lower temperatures. In addition, when employing electrodeposition method, there is possibility of presence of fine nanoparticles in our samples. At room temperature these nanoparticles are super-paramagnetic in nature but at lower temperatures, when they are in blocking state, they efficiently contribute to the overall magnetization of nanostructures resulting an enhancement in M_s.[36] Fig. 5d shows the temperature dependent variation in H_c and H_{ex} after the sample being field cooled. Increased H_c values are observed with the decrease in temperature which is due to the thermal relaxation over the anisotropy energy barrier. The highest H_{ex} value of 77 Oe has been observed at 5 K followed by a decrease which can be attributed to the thermally induced loss of magnetic stability of the antiferromagneitc spin order at the interface of BLFO shell and CoPt core.[37,38]

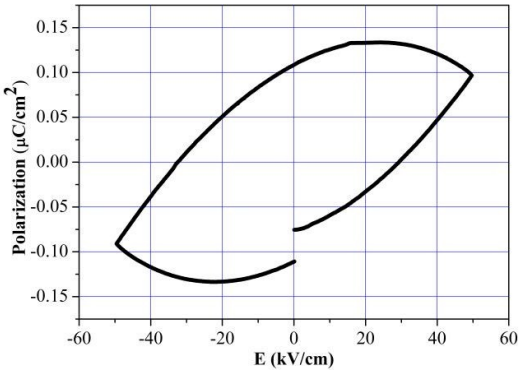

Fig. 6 Room temperature ferroelectric P (E) loop of BLFO NTs.

The room temperature ferroelectric (P-E) hysteresis loop of BLFO NTs is shown in Fig. 6. The true realization of ferroelectric behaviour of materials with such P-E loops can be challenging and misleading sometimes particularly in the field of multiferroics where P-E hysteresis loops for materials such as BFO are often dominated by leakage current mainly due to mixed valence for the magnetic ions Fe^{2+} and Fe^{3+}, from oxygen vacancies, or from both [Fig. S4†]. It has already been reported that matrials that exhibit saturation in polarization and have concave region in P-E loop are the true ferroelectrics.[39] A clear saturation polarization and concave region in P-E loop can be seen in Fig. 6, giving an indication for the presence of intrinsic ferroelectricity in BLFO NTs sample. The charge defects such as bismuth and oxygen vacancies (Vo) are the main culprit behind the high conductivity in pure BFO ceramics. The oxygen vacancies generated due to Bi volatility and Fe^{3+} to Fe^{2+} transition carry a positive charge and attract electrons from Fe^{2+} ions which possibly leads to hop of electron towards Fe^{3+} resulting high conductivity and leakage current in pure BFO. Therefore replacement of highly volatile Bi with La reduces the concentration of Vo giving reduced leakage current and improved P-E loop.[40]

Conclusions

In conlcusion, a new hybrid core-shell $Co_{90}Pt_{10}$-$Bi_{0.87}La_{0.13}FeO_3$ 1D NWs geometry has been reported with ferromagnetic core and multiferroic shell synthesized by a three-step fabrication methodology. Multiferroic $Bi_{0.87}La_{0.13}FeO_3$ shell has been grown by sol-gel method in AAO template with pore diameter of 120 nm followed by the potentiostatic electrodeposition of $Co_{90}Pt_{10}$ core inside the BLFO shell. La doping significantly reduces the presence of other more stable phases of bismuth ferrite giving polycrystalline single-phase BLFO NTs. Magnetic properties measurements at room temperature show the easy magnetization axis along the NWs owing to the stronger shape anisotropy. Angular dependent behaviour of H_c shows a switching in magnetization reversal mechanism from curling rotation to coherent rotation. Multifunctionality of BLFO has been observed by the coexistence of ferroelectric and anti-ferromagnetic spin ordering demonstrated by the electric polarization P-E loop and exchange bias effect. The room temperature existence of exchange bias without annealing treatment is attributed to the rearrangement of anti-ferromagnetic domains in BLFO shell during the electrodeposition of CoPt core giving a clear indication of exchanged coupling between the ferromagnetic core and anti-ferromagnetic BLFO shell. Furthermore, at lower temperature, the reduced thermal fluctuations, existence of superparamagnetic nanoparticles in blocking state and thermal relaxation over the anisotropy energy barrier are the major factors to effect the coercivity and exchange bias. This insight study of multifucntional BLFO shell and ferromagnetic CoPt core gives a realization of magnetoelectric coupling in 1D composite materials, i.e. a magnetic response to an electric field and vice versa. In addition, this low cost method can be easily employed to fabrication and study of other hybrid nanostructures giving a vast room of investigation to researchers.

Acknowledgements

This work was supported by State Key Project of Fundamental Research of Ministry of Science and Technology [MOST, No. 2010CB934401] and the National Natural Science Foundation [NSFC, Grant No. 11374351, and 11434014], and the partial support of NSFC-JSPS Scientific Cooperation Program.

References

1 T. N. Narayanan, B. P. Mandal, A. K. Tyagi, A. Kumarasiri, X. Zhan, M. G. Hahm, M. R. Anantharaman, G. Lawes and P. M. Ajayan, *Nano Lett.,* 2012, **12**, 3025.
2 A. Bruce, B. Scrosati, T. J. Marie and W. V. Schalkwijk, *Nat. Mater.,* 2005, **4**, 366.
3 R. Gasparac, P. Kohli, M. O. Mota, L. Trofin and C. R. Martin, *Nano Lett.,* 2004, **4**, 513.
4 S. R. Gowda, A. L. M. Reddy, X. Zhan and P. M. Ajayan, *Nano Lett.,* 2011, **11** (8), 3329.
5 A. Kros, R. J. M. Nolte and N. A. J. M. Sommerdijk, *Adv. Mater.,* 2002, **14**, 1779.
6 S. Shamaila, D. P. Liu, R. Sharif, J. Y. Chen, H. R. Liu and X. F. Han, *Appl. Phys. Lett.,* 2009, **94**, 203101.
7 S. S. Ali, K. Javed, D. W. Shi, L. L. Tao, J. Jiang, G. J. Zhai and X. F. Han, *J. Appl. Phys.,* 2014, **115**, 17A762.
8 M. Dawber, K. M. Rabe and J. F. Scott, *Rev. Mod. Phys.,* 2005, **77**, 1083.
9 J. Ma, J. Hu, Z. Li and C. W. Nan, *Adv. Mater.,* 2011, **23**, 1062.
10 D. W. Shi, K. Javed, S. S. Ali, J. Y. Chen, P. S. Li, Y. G. Zhao and X. F. Han, *Nanoscale,* 2014, **6**, 7215.
11 H. Bea, M. Bibes, A Barthélémy, K. Bouzehouane, E. Jacquet, A. Khodan and J. P. Contour, *Appl. Phys. Lett.,* 2005, **87**, 072508.
12 M. Valant, A. K. Axelsson and N. Alford, *Chem. Mater.,* 2007, **19**, 5431.
13 G. Catalan and J. F. Scott, *Adv. Mater.,* 2009, **21**, 2463.
14 C. Ederer and N. A. Spaldin, *Phys. Rev. B,* 2005, **71**, 060401(R).
15 M. Lorenz, V. Lazenka, P. Schwinkendorf, F. Bern, M. Ziese, H. Modarresi, A. Volodin, M. J. Van Bael, K. Temst, A. Vantomme and M. Grundmann, *J. Phys. D: Appl. Phys.,* 2014, **47**, 135303.
16 Y. H. Lin, Q. Jiang, Y. Wang, C. W. Nan, L. Chen and J. Yu, *Appl. Phys. Lett.,* 2007, **90**, 172507.
17 G. L. Bras, D. Colson, A. Forget, N. G. Riondet, R. Tourbot and P. Bonville, *Phys. Rev. B,* 2009, **80**, 134417.
18 I. Levin, S. Karimi, V. Provenzano, C. L. Dennis, H. Wu, T. P. Comyn, T. J. Stevenson, R. I. Smith and I. M. Reaney, *Phys. Rev. B,* 2010, **81**, 020103 (R).
19 S. B. Emery, C. J. Cheng, D. Kan, F. J. Rueckert, S. P. Alpay, V. Nagarajan, I. T. keuchi and B. O. Wells, *Appl. Phys. Lett.,* 2010, **97**, 152902.
20 A. Chen, H. Zhou, Z. Bi, Y. Zhu, Z. Luo, A. Bayraktaroglu, J. Phillips, E. M. Choi, J. L. MacManus-Driscoll, S. J. Pennycook, J. Narayan, Q. Jia, X. Zhang and H. Wang, *Adv. Mater.,* 2013, **25**, 1028.
21 I. Sosnowska, T. P. Neumaier and Steichele, *J. Phys. C: Solid State Phys.,* 1982, **15**, 4835.
22 Reetu, A. Agarwal, S. Sanghi, Ashima and N. Ahlawat, *J. Phys. D: Appl. Phys.,* 2012, **45**, 165001.
23 T. Zhao, A. Scholl, F. Zavaliche, K. Lee, M. Barry, A. Doran, M. P. Cruz, Y. H. Chu, C. Ederer, N. A. Spaldin, R. R. Das, D. M. Kim, S. H. Baek, C. B. Eom and R. Ramesh, *Nat. Mater.,* 2006, **5**, 823.
24 C. Binek and B. Doudin, *J. Phys.: Condens. Matter,* 2005, **17**, L39.

25 P. Borisov, A. Hochstrat, X. Chen, W. Kleemann and *C. Binek, Phys. Rev. Lett.,* 2005, **94**, 117203.
26 H. Béa, M. Gajek, M. Bibes and A. Barthélémy, *J. Phys.: Condens. Matter,* 2008, **20**, 434221.
27 X. Y. Zhang, G. H. Wen, Y. F. Chan, R. K. Zheng, X. X. Zhang and N. Wang, *Appl. Phys. Lett.,* 2003, **83**, 3341.
28 D. H. Qin, L. Cao, Q. Y. Sun, Y. Huang and H. L. Li, *Chem. Phys. Lett.,* 2002, **358**, 8484.
29 F. M. F. Rhen, E. Backen and J. M. D. Coey, *J. Appl. Phys.,* 2005, **97**, 113908.
30 J. Y. Chen H. R. Liu, N. Ahmad, Y. L. Li, Z. Y. Chen, W. P. Zhou and X. F. Han, *J. Appl. Phys.,* 2011, **109**, 07E157.
31 G. C. Han B. Y. Zong, P. Luo and Y. H. Wu, *J. Appl. Phys.,* 2003, **93**, 9202.
32 X. F. Han, S. Shamaila, R. Sharif, J. Y. Chen, H. R. Liu and D. P. Liu, *Adv. Mater.,* 2009, **21**, 4619.
33 L. Sun, Y. Hao, C. L. Chien and P. C. Searson, *IBM J. Res. Dev.,* 2005, **49**, 79.
34 E. C. Stoner and E. P. Wohlfarth, *Phil. Trans. Roy. Soc.,* 1948, **A240**, 599.
35 M. P. Proenca, J. Ventura, C. T. Sousa, M. Vazquez and J. P. Araujo, *Phys. Rev. B,* 2013, **87**, 134404.
36 J. Y. Chen, N. Ahmad, D. W. Shi, W. P. Zhou and X. F. Han, *J. Appl. Phys.,* 2011, **110**, 073912.
37 S. Shamaila, R. Sharif, S. Riaz, M. Ma, M. Khaleeq-ur-Rahman and X. F. Han, *J. Magn. Magn. Mater.,* 2008, **320**, 1803.
38 J. Sort,V. Langlais, S. Doppiu, B. Dieny, S. Surinach, J. S. Munoz, M. D. Baró, C. H. Laurent and J. Nogués, *Nanotechnology*, 2004, **15**, S211.
39 J. F. Scott, *J. Phys.: Condens. Matter,* 2008, **20**, 021001.
40 B. H. Park, B. S. Kang, S. D. Bu, T. W. Noh, J. Lee and W. Jo, *Nature,* 1999, **401**, 682.